World Academy of Science, Engineering and Technology
International Journal of Energy and Power Engineering
Vol:15, No:6, 2021

Lead-Free Inorganic Cesium Tin-Germanium Triiodide Perovskites for Photovoltaic Application

Seyedeh Mozhgan Seyed-Talebi, Javad Beheshtian

***Abstract*—**The toxicity of lead associated with the lifecycle of perovskite solar cells (PSCs) is a serious concern which may prove to be a major hurdle in the path toward their commercialization. The current proposed lead-free PSCs including Ag(I), Bi(III), Sb(III), Ti(IV), Ge(II), and Sn(II) low-toxicity cations are still plagued with the critical issues of poor stability and low efficiency. This is mainly because of their chemical stability. In the present research, utilization of all inorganic $CsSnGeI_3$ based materials offers the advantages to enhance resistance of device to degradation, reduce the cost of cells, and minimize the carrier recombination. The presence of inorganic halide perovskite improves the photovoltaic parameters of PCSs via improved surface coverage and stability. The inverted structure of simulated devices using a 1D simulator like solar cell capacitance simulator (SCAPS) version 3308 involves TCOHTL/Perovskite/ETL/Au contact layer. PEDOT:PSS, PCBM, and $CsSnGeI_3$ used as hole transporting layer (HTL), electron transporting layer (ETL), and perovskite absorber layer in the inverted structure for the first time. The holes are injected from highly stable and air tolerant $Sn_{0.5}Ge_{0.5}I_3$ perovskite composition to HTM and electrons from the perovskite to ETL. Simulation results revealed a great dependence of power conversion efficiency (PCE) on the thickness and defect density of perovskite layer. Here the effect of an increase in operating temperature from 300 K to 400 K on the performance of $CsSnGeI_3$ based perovskite devices is investigated. Comparison between simulated $CsSnGeI_3$ based PCSs and similar real testified devices with spiro-OMeTAD as HTL showed that the extraction of carriers at the interfaces of perovskite absorber depends on the energy level mismatches between perovskite and HTL/ETL. We believe that optimization results reported here represent a critical avenue for fabricating the stable, low-cost, efficient, and eco-friendly all-inorganic Cs-Sn-Ge based lead-free perovskite devices.

***Keywords*—**Hole transporting layer, lead-free, perovskite Solar cell, SCAPS-1D, Sn-Ge based material.

I. Introduction

THE toxicity of lead in halide perovskite is a serious issue in high efficiency PSCs, however current lead-free PSCs are still plagued with the serious problems of low efficiency and poor stability [1]. Among intensive efforts to find more stable lead-free PSC candidates, Sn(II) based halide perovskites endowed with appropriate light absorption (1.81-1.92 eV), have revealed the highest efficiency as promising materials for photovoltaic applications [2]. Although, considered Sn-based PSCs include $CH_3NH_3SnI_3$ ($MASnI_3$), and $HC(NH_2)_2SnI_3$ ($FASnI_3$) have been presented to deliver high efficiency, up to 9%, these materials have intrinsically low stability [3], [4]. Instability of these Sn(II) based halide perovskites is attributed to the presence of the organic cations [5]. From this point of view, the all-inorganic lead-free $CsSnI_3$ based PSCs become more attractive candidates due to their high intrinsic or thermodynamic stability, and small band gap (about 1.3 eV) combined with high optical absorption coefficient. Unfortunately, the resulting PSCs have been presented maximum PCE of only 4.81%, and no operational stability data on these PSCs have been reported because of the high defect density attributed to the easy oxidation of divalent Sn^{2+} to Sn^{4+} or Sn vacancies in the bulk and surfaces of $CsSnI_3$ perovskite absorber [6]-[11]. One of the most effective strategies that have been proposed for exerting control over charge carrier lifetime, Sn oxidation, and defect/trap density recombination in $CsSnI_3$-based PSCs is to alloy Ge(II) in $CsSnI_3$ to form a $CsSn_{0.5}Ge_{0.5}I_3$ perovskite composition. The extraordinary stability of the $CsSn_{0.5}Ge_{0.5}I_3$ based perovskite is explained using experiments upon continuous operation under 1-sun illumination for over 500 h [12]. By exposing the $CsSn_{0.5}Ge_{0.5}I_3$ perovskite layer to air, a stable native-oxide layer forms on the surface, within 30 s, leading to increase the PCE of inorganic lead-free PSCs up to 7.11%. Thus, based on the knowledge gained from these studies, in the present research, the stable and air tolerant $CsSn_{0.5}Ge_{0.5}I_3$ composition is used as a perovskite absorber in simulated devices.

Seyedeh Mozhgan Seyed-Talebi is with the Shahid Rajaee Teacher Training University, Iran, Islamic Republic Of (e-mail: m.seyedtalebi@sru.ac.ir).

II. Theoretical Methods and Device Structure

Device simulation is a valuable tool that can provide useful information for understanding device operation mechanism and design optimum layer configuration to improve the photovoltaic parameters of PSCs to be characterized experimentally. The theoretical and experimental characterization results exhibited a reasonable agreement for simulation of tin based PSCs with 1D simulator like SCAPS [13]. In the present study, we used SCAPS version 3308 for our simulation platform. In SCAPS software a solar cell device is defined as the number of semiconductor layers, in which the transportation of electrons and holes are considered by solving the continuity and Poisson's equations governing the carriers.

A. Device Structure

The inverted structure of simulated devices, which is usually used to calculate the photovoltaic parameters of PSCs, involves TCO/HTL/Perovskite/ETL/Au back contact. A typical architecture of our simulated $CsSnGeI_3$ based devices is presented schematically in Fig. 1. PEDOT: PSS, PCBM, and $CsSnGeI_3$ are used as the HTL, ETL, and perovskite

active layer, respectively. Furthermore, an interface defect layer (IDL) is inserted for the passivation of the interfacial recombination centers and the suppression of current leakage at the interface between the $CsSnGeI_3$ and PCBM layer.

As the extraction of carriers at the interfaces of the perovskite absorber depends on the energy level mismatches between the perovskite and HTL/ETL. The energy level values are essential factors that affect the efficiency of devices [14], [15]. The energy band diagrams and levels of the simulated $CsSnGeI_3$ based PSCs are presented in Fig. 2.

Due to excellent film forming properties, high transparency, easy processing condition under ambient atmosphere at low temperature (< 150 °C), PEDOT:PSS has been widely used as a HTL in real devices. Utilizing PEDOT:PSS as a HTL in $CsSn_{0.5}Ge_{0.5}I_3$ based PSCs reported here for the first time. Energy level mismatch of PEDOT:PSS with perovskite absorber is a critical issue for determining the open-circuit voltage and carrier recombination at the interface. Therefore, typical inverted mixed halide PSCs ($CsSnGeI_3$) with PEDOT: PSS as a HTL exhibited relatively low open circuit voltage (V_{oc}). Despite the mentioned fact, optimization results of the perovskite layer will be useful for choosing new ETMs/HTMs in simulated $CsSnGeI_3$ based PSCs by worldwide researchers. The C60 was utilized here to increase the electron mobility and electrical conductivity of PCBM [16]. For higher efficiency and improvement in transporting the photo-generated carriers, a modification is necessary to decrease the interfacial energy loss.

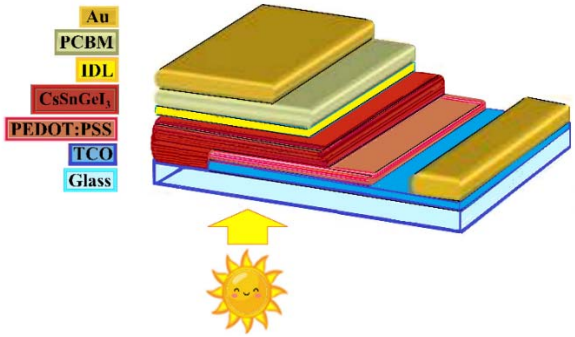

Fig. 1 The final model of the proposed nanostructured PSC

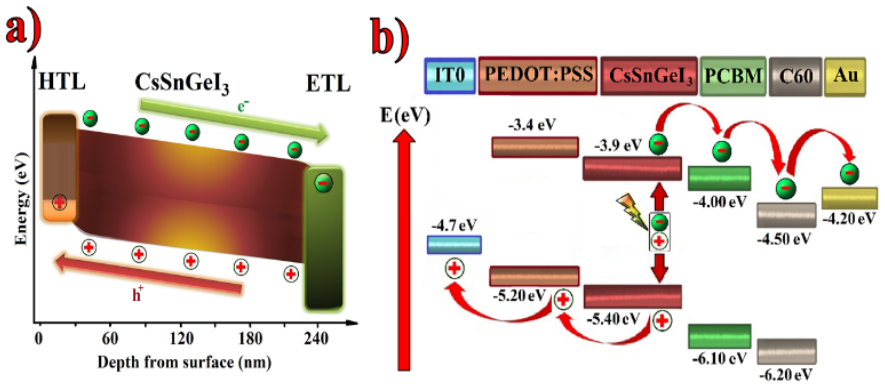

Fig. 2. (a) The energy band diagrams, and (b) corresponding conduction and valence band positions of simulated $CsSnGeI_3$ based PSCs layers

TABLE I
INPUT PARAMETERS OF SIMULATED $CsSnGeI_3$ BASED SOLAR CELL AT 300 K UNDER AM 1.5 G ONE-SUN OF ILLUMINATION (100 MW/CM^2)

Parameters	PEDOT:PSS	$CsSnGeI_3$	PCBM	C60
Thickness (nm)	30	200	25	20
E_g (eV)	1.8	1.5	2.1	1.7
χ(eV)	3.40	3.9	4.039	4.5
ε_r	18.0	28.0	18.0	18.0
N_c (cm^{-3})	$2.2\times10^{+18}$	$2.2\times10^{+18}$	$2.2\times10^{+18}$	$2.2\times10^{+18}$
N_v (cm^{-3})	$1.8\times10^{+19}$	$1.8\times10^{+19}$	$1.8\times10^{+19}$	$1.8\times10^{+19}$
V_e/V_p (cm/s)	10^7	10^7	10^7	10^7
μ_n (cm^2/Vs)	4.5×10^{-2}	9.74×10^{2}	2×10^{-3}	8×10^{-2}
μ_p (cm^2/Vs)	4.5×10^{-2}	2.13×10^{2}	2×10^{-3}	8×10^{-2}
N_D (cm^{-3})	0	10^{+13}	10^{+17}	10^{+18}
N_A (cm^{-3})	10^{+20}	0	0	0
σ_e and σ_p	2×10^{-14}	2×10^{-14}	2×10^{-14}	2×10^{-14}
N_t (cm^{-3})	10^{+15}	$1\times10^{+16}$	10^{+15}	10^{+15}

The exact values of the physical parameters for new materials are difficult to obtain, the main material parameters in this study are carefully selected from those testified in other theoretical and experimental reports [12], [17]. Table I recapitulates all the primary parameters and defects of each layer used in the current simulation. Here, E_g is band gap energy, χ is electron affinity, ε_r is relative permittivity, N_c and N_v indicate effective density of states of conduction band and valence band, N_A and N_D denote acceptor and donor densities, μ_n and μ_p are mobilities of electron and hole, σ_e and σ_p are capture cross section of electron and hole, and N_t assumed as amount of defect density to obtain 1 µm for carrier diffusion lengths of electron and hole (L_n and L_p), which is a similar value to the experiment [12].

III. RESULTS AND DISCUSSIONS

Figs. 3 (a) and (b) present the J–V response scan and quantum efficiency spectra of optimized device, respectively. The promising efficiency of 5.64% is achieved for all-inorganic $CsSnGeI_3$ PSC through the mentioned structure in Fig. 1. In this simulation, about 200 nm thickness of $CsSnGeI_3$ thin film (as reported in real fabricated devices) is sandwiched between PEDOT:PSS as a HTL and PCBM as ETL, with the thin native layer serving as an interfacial layer between the

$CsSn_{0.5}Ge_{0.5}I_3$ perovskite layer and the HTL.

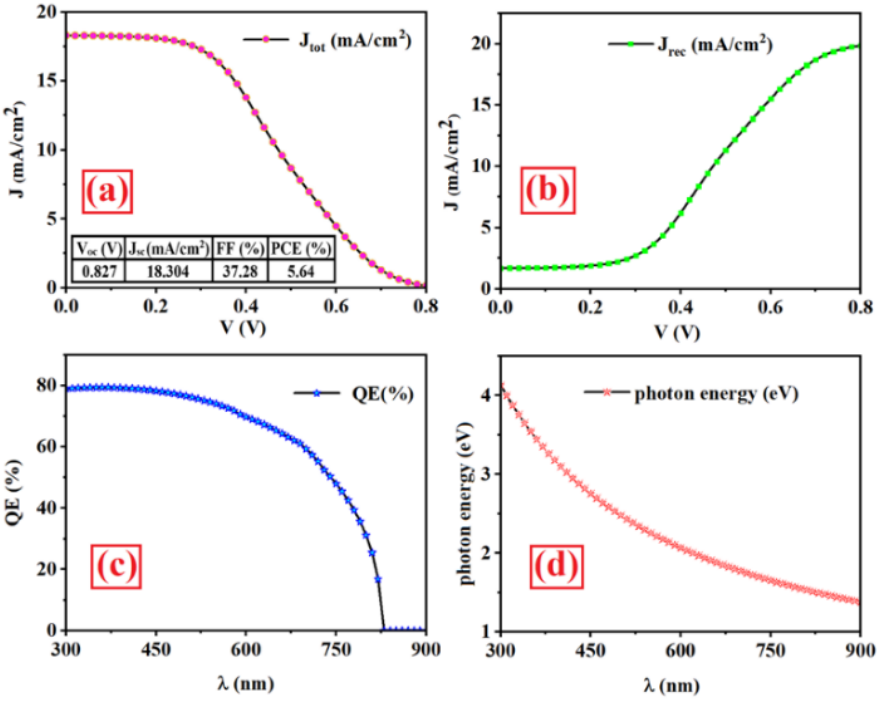

Fig. 3 (a) Photocurrent density-Voltage characteristic, (b) total recombination current density, (quantum efficiency, and (d) photon energy of the simulated $CsSnGeI_3$ based solar cell with PEDOT:PSS thickness of 20 nm and PCBM layer thickness of 20 nm. The input light power was based on air mass (AM) 1.5 G spectrum

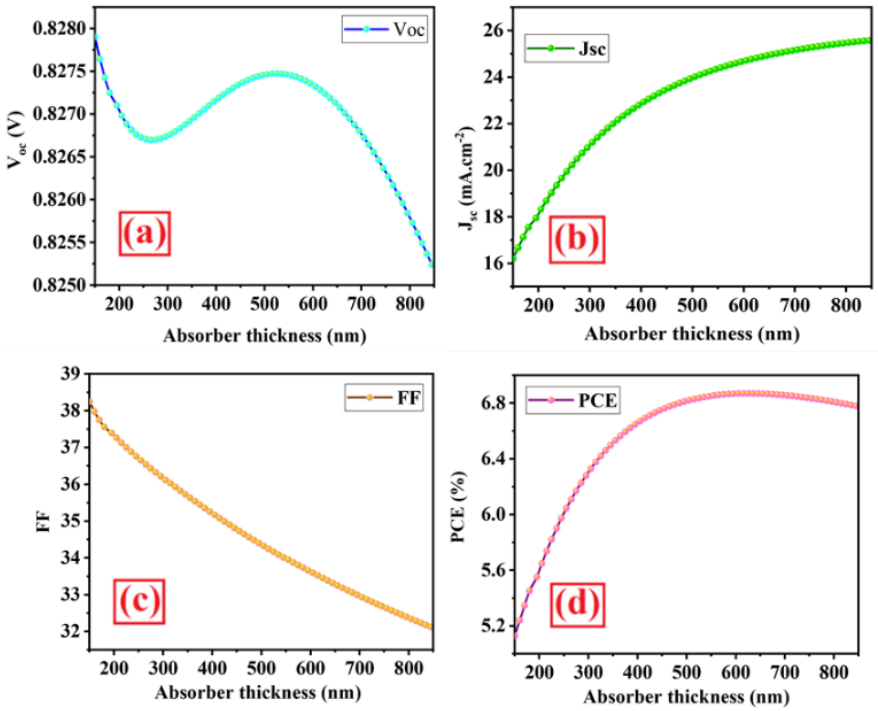

Fig. 4 Photocurrent density-Voltage characteristic of the device with modified $CsSnGeI_3$ thickness of 150-850 nm. The input light power was based on AM 1.5 G spectrum

The carrier recombination across the device is attributable not only to the defect density, but also more importantly to the conduction band offset between the HTL/ETL and perovskite layer. Loss of charge carriers occurred here because of the existing mismatch between the energy levels of PEDOT:PSS and perovskite absorber. In comparison to experimental results

of all-inorganic $CsSnGeI_3$ with 200 nm thickness of the perovskite absorber device and spiro-OMeTAD HTL, it was found that both extraction and injection barriers of PEDOT: PSS are not as good as spiro-OMiTAD to PSC efficiency [12]. Here, the extraction barrier resulted from existing mismatch influenced the fill factor with no obvious effect on the device V_{oc}. Increase of recombination at contacts and decreasing the carrier's extraction in the cell reduce the photon energy and efficiency of PSC.

A. Effect of the Absorber Thickness

At first, the present research focuses on the dependence of the spectral response of the devices on the modification of perovskite absorber thickness which has great importance in determining the more efficient devices. Although, the initial thickness of 200 nm is considered for the simulated $CsSnGeI_3$ perovskite layer according to a previous experimental report, the optimum thickness range of 500 nm resulted from the simulation using SCAPS software [12]. By increasing the thickness of the absorber from 100 nm to 500 nm, the number of photo-generated carriers and consequently the output current density and its corresponding PCE of the device, improved due to increased light absorption.

The results of Fig. 5 show that when the thickness is greater than 500 nm, J_{sc} will saturate to a maximum value and fluctuate in small-amplitude with increased thickness. Therefore, a device based on the thickness of 500 nm for $CsSnGeI_3$ yielded the highest PCE of about 6.8%.

To verify the applicability of our approach, a $CsSn_{0.5}Ge_{0.5}I_3$ based device also simulated with the tested HTL (Spiro-OMeTAD) and ETL (PCBM), the efficiency jumped from 7.11% (reported in real experiment) for thickness of 200 nm to 9.58% (V_{oc} = 0.97 V, J_{sc}= 16.83 mA/cm^2, FF = 58.53%) for our optimum thickness of 500 nm [12].

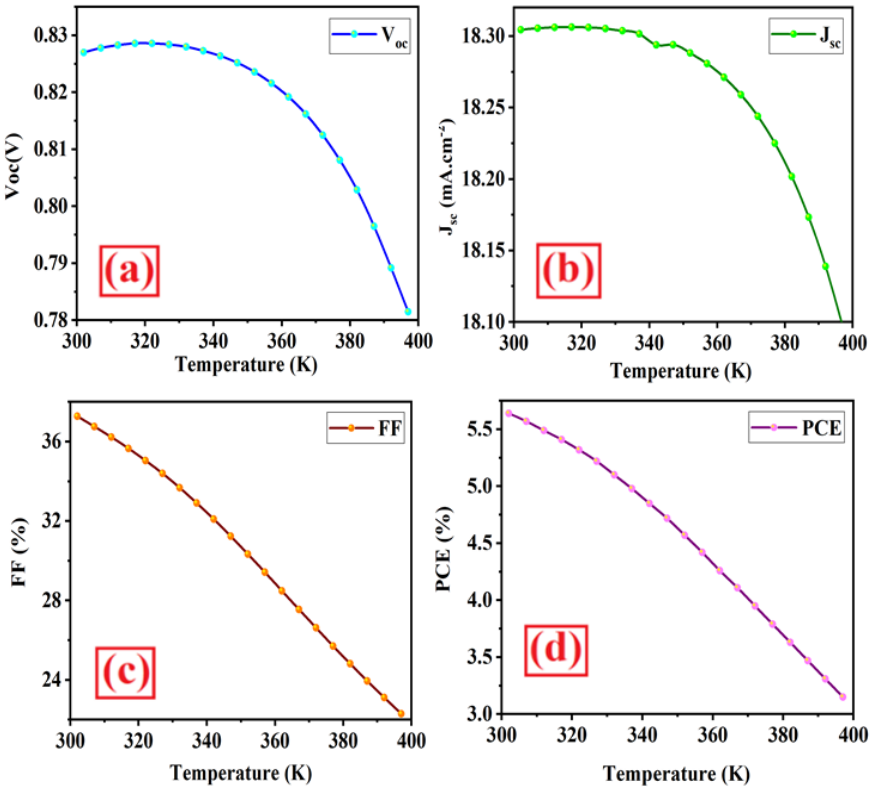

Fig. 5 Results of change in the photovoltaic parameters of $CsSnGeI_3$ based devices include (a) open circuit voltage, (b) short circuit current density, (c) fill factor, and (d) efficiency characteristics as a function of temperature modification from 300 K to 400 K. The irradiance of 1000 W/m^2 with AM 1.5G is applied to devices

B. Effect of Temperature on the Photovoltaic Parameters

In standard test conditions for photovoltaic cells, the devices are characterized under temperature of 300 K (25 °C), solar radiation of 1000 W/m^2, and air mass 1.5 G. Thus, in the present simulation, the working temperature is set to 300 K. In real conditions by increasing the cell temperature, the mobility of carriers and their concentrations get extremely influenced as the temperature changed which results in poor efficiency. Therefore, modification of the local temperature is considered in the current simulation to make it closer to the real conditions. To investigate how working temperature affects the photovoltaic parameters of devices, it is varied from 300 K to 400 K. In Fig. 5 (a), the variation in solar cell parameters according to the modifications in the operating temperature are depicted. At 300 K the simulation resulted in V_{OC} of 0.827 V, J_{SC} of 18.30 mA/cm^2, FF of 37.28%, and PCE of 5.64%. As the temperature rises towards 400 K, the simulation results in V_{OC} 0.781 V, J_{SC} 18.09 mA/cm^2, FF 22.3%, PCE 3.15%. By

increasing the temperature, increased stress and strain result in distortion and disorder in the absorber layer. Pin-holes take this situation to new level and uninvited recombination occurs that cost in enhancement of resistance and finally, it minifies the efficiency of the device. Therefore, the best photovoltaic performance is achieved at 300 K.

C. Effect of Defect Density of Absorber (N_t)

The amount of defects in the perovskite absorber plays an important role in determining the PCE of the devices. As the photo carriers generated in this layer, the charge recombination behaviors can become dominant in determining the V_{oc}, J_{sc}, FF, and PCE of the device. Despite the difficulty in quantifying the recombination rate in real devices, in our simulation the defect density changed drastically from 1×10^{12} cm^3 to 1×10^{19} cm^3 to reveal the importance of perovskite layer quality. The effect of defect density changes of the $CsSnGeI_3$ layer on the J-V curves and QE of devices is shown in Fig. 6.

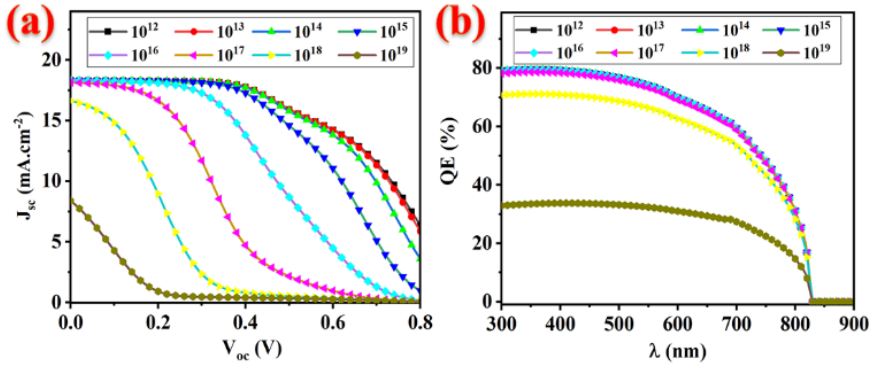

Fig. 6 Modification of (a) J-V characteristics, and (b) Quantum efficiency of devices with the defect density changes of the $CsSnGeI_3$ perovskite layer from 1×10^{12} cm^3 to 1×10^{19} cm^3

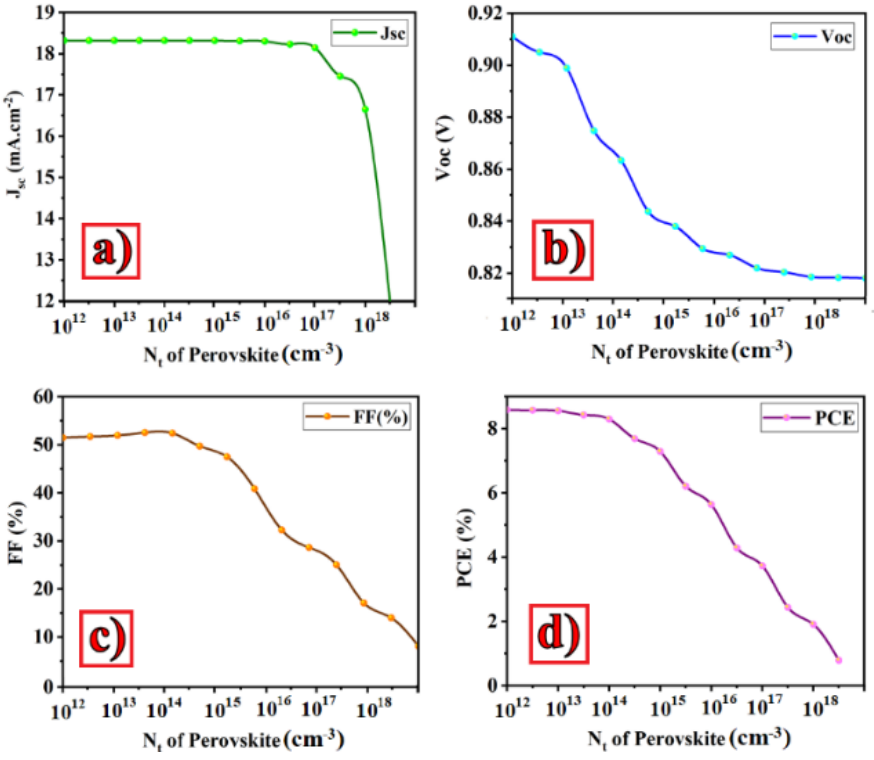

Fig. 7 The relationship between the defect density of the $CsSnGeI_3$ perovskite layer and photovoltaic parameters of devices include (a) short circuit current density, (b) open circuit voltage, (c) fill factor, and (d) efficiency

The presence of the defect states in the perovskite layer causes an extensive drop in all photovoltaic parameters. Increasing the defect density of the perovskite absorber from 1×10^{12} cm^3 to 1×10^{19} cm^3 resulted in a drop in efficiency from 8.59% to 0.43%. According to the simulation results, reducing the bulk defect density of the $CsSnGeI_3$ layer to the order of ~10^{13} cm^{-3} is necessary and urgently needed in experimental samples. The variation curves of photovoltaic

parameters as a function of trap density in the perovskite layer is shown in Fig. 7.

The mentioned results are in agreement with the fact that the high crystallinity of the perovskite helps to minimize the trap density and charge recombination within perovskite, and hence allows high efficiency to be obtained. Therefore, it is expected that improvement in the growth process of perovskite layers can enhance device efficiency.

IV. Conclusion

Simulation of $CsSnGeI_3$ based PSCs was performed using SCAPS software for the first time. The thickness and defect density of perovskite layers was optimized. To investigate the effect of energy mismatch reduction on minimizing the energy loss at the interfaces, and to check the optimized thickness of $CsSnGeI_3$, reported, a real $CsSnGeI_3$ based device with spiro-OMeTAD HTL simulated. The photovoltaic parameters of the simulated device were completely in agreement with the experimental results. By utilizing the optimized thickness of 500 nm for the perovskite layer, efficiency enhanced from 7.11% to 9.58%. Therefore, the optimized thickness of 500 nm proposes for the $CsSnGeI_3$ based perovskite layer to have more efficient PCSs. Furthermore, the modification of local temperature is considered in the current simulation to make it closer to the real conditions and to understand its impact on the photovoltaic parameters. With the increase of the temperature from 300 K to 400 K, the PCE of the cells dropped from 8.59% to 0.43%.

Acknowledgment

The authors would like to acknowledge Dr. Marc Burgelman (University of Gent) for providing SCAPS software. Acknowledgment also goes to Shahid Rajaee University for providing the opportunity to carry out the research work.

References

[1] S. Nair, S. B. Patel, and J. V. Gohel, "Recent trends in efficiency-stability improvement in perovskite solar cells", *Mater. Today Energy*, 2020, 17, 100449.

[2] Y. Zhou, and Y. Zhao, "Chemical stability and instability of inorganic halide perovskites," *Energy Environ. Sci.*, 2019, 12, pp. 1495-1511.

[3] S. Shao, J. Liu, G. Portale, H. -H. Fang, G. R. Blake, G. H. Brink, L. J. Anton Koster, and M. A. Loi, "Highly reproducible Sn-based hybrid perovskite solar cells with 9% efficiency", *Adv. Energy Mater.*, 2018, 8, 1702019.

[4] L. Peng, and W. Xie, Theoretical and experimental investigations on the bulk photovoltaic effect in lead-free perovskites $MASnI_3$ and $FASnI_3$, *RSC Adv.*, 2020, 10, pp. 14679-14688.

[5] B. Kima, and S. I. Seok, "Molecular aspects of organic cations affecting the humidity stability of perovskites," *Energy Environ. Sci.*, 2020, 13, pp. 805-820.

[6] T. Handa, T. Yamada, H. Kubota, S. Ise, Y. Miyamoto, Y. Kanemitsu, "Photocarrier recombination and injection dynamics in long-term stable lead-free $CH_3NH_3SnI_3$ perovskite thin films and solar cells, " *J. Phys. Chem. C.*, 2017, 121, pp. 16158–16165.

[7] T. Bin Song, T. Yokoyama, S. Aramaki and M. G. Kanatzidis, "Performance Enhancement of Lead-Free Tin-Based Perovskite Solar Cells with Reducing Atmosphere-Assisted Dispersible Additive," *ACS Energy Lett*, 2017, 2 (4), pp. 897-903.

[8] T. Zhang, H. Li, H. Ban, Q. Sun, Y. Shen, and M. Wang, "Efficient $CsSnI_3$-based inorganic perovskite solar cells based on mesoscopic metal oxide framework via incorporating donor element," *J. Mater. Chem. A*, 2020, 8 (7), pp. 4118-4124.

[9] N. Wang, Y. Zhou, M. G. Ju, H. F. Garces, T. Ding, S. Pang, X. C. Zeng, N. P. Padture, and X. W. Sun, "Heterojunction-Depleted Lead-Free Perovskite Solar Cells with Coarse-Grained B-γ-$CsSnI_3$ Thin Films," *Adv. Energy Mater.* 2016, 6(24), 1601130.

[10] G. E. Eperon, G. M. Paternò, R. J. Sutton, A. Zampetti, A. A. Haghighirad, F. Cacialli, and H. J. Snaith, "Inorganic Cesium Lead Iodide Perovskite Solar Cells, " *J. Mater. Chem. A*, 2015, 3, pp. 19688-19695.

[11] P. Luo, W. Xia, S. Zhou, L. Sun, J. Cheng, C. Xu, and Y. Lu, "Solvent Engineering for an Ambient-Air-Processed, Phase-Stable $CsPbI_3$ in Perovskite Solar Cells," *J. Phys. Chem. Lett*. 2016, 7 (18), pp. 3603-3608.

[12] M. Chen, M. -G. Ju, H. F. Garces, A. D. Carl, L. K. Ono, Z. Hawash, Y. Zhang, T. Shen, Y. Qi, R. L. Grimm, D. Pacifici, X. C. Zeng, Y. Zhou, and N. P. Padture, "Highly stable and efficient all-inorganic lead-free perovskite solar cells with native-oxide passivation," *Nature Communications*, 2019, 10, 16.

[13] M. Burgelman, P. Nollet, S. Degrave, "Modeling polycrystalline semiconductor solar cells," *Thin Solid Films*, 2000, 527, pp. 361–362.

[14] S. Shao, and M. A. Loi, "The Role of the Interfaces in Perovskite Solar Cells, *ADV. Mater. Interfaces*," 2020, 7(1), 1901469.

[15] S. Wang, T. Sakurai, W. Wen, Y. Qi, "Energy Level Alignment at Interfaces in Metal Halide Perovskite Solar Cells," *Adv. Mater. Interfaces*, 2018, 5(22):1800260.

[16] A. Al Mamun, T. T. Ava, K. Zhang, H. Baumgart, and G. Namkoong, "New PCBM/carbon based electron transport layer for perovskite solar cells, " *Phys. Chem. Chem. Phys.*, 2017, 19, 17960.

[17] M. B. Faheem, B. Khan, C. Feng, M. U. Farooq, F. Raziq, Y. Xiao, and Y. Li, "All-Inorganic Perovskite Solar Cells: Energetics, Key Challenges, and Strategies toward Commercialization," *ACS Energy Lett*. 2020, 5, pp. 290−320.